

EFFECTS OF NICKEL CONTENTS ON PHASE CONSTITUENT AND MECHANICAL PROPERTIES OF DUCTILE IRON

Xin Wang, Yuzhou Du , Ruochen Zhang, Chen Liu, Xiaoyu Mei, Xinyu Yang and Bailing Jiang

School of Materials Science and Engineering, Xi'an University of Technology, Xi'an 710048, People's Republic of China

Copyright © 2023 American Foundry Society
<https://doi.org/10.1007/s40962-023-01208-1>

Abstract

Ductile iron with different Ni contents (0–10%) was successfully fabricated through horizontal continuous casting technology, and the effects of Ni content on ductile iron's microstructure and mechanical properties were investigated. The results showed that the Ni addition affected the diffusion of carbon atoms, altering the phase constituents during solid-state transformation. The ductile iron with Ni amounts less than 2% was composed of spheroidal graphite and ferrite. The addition of the 2% Ni addition led to more than 40% pearlite in the matrix. When the Ni content exceeded 6%, bainite and martensite were detected, which

enhanced strength significantly but deteriorated ductility. Annealing treatment facilitated the dissolution of carbides and increased ferrite fraction, contributing to the improvement of ductility. The as-annealed sample with 8% Ni showed an ultimate tensile strength of 1057 MPa and an elongation of 4.6%.

Keywords: ductile iron, Ni addition, annealing treatment, acicular structure, mechanical properties

Introduction

Ductile iron is widely used in automotive, agricultural, and other industries because of its good mechanical properties, machinability, and low cost.¹ The mechanical properties of ductile iron can be optimized through heat treatment.^{2,3} For example, a very fine ferrite matrix was obtained in ductile iron by intercritical quenching and annealing treatment, which effectively improved the strength.⁴ Additionally, austempering heat treatment was commonly used to produce a unique matrix microstructure consisting of acicular ferrite (α) and high carbon austenite (γ) to enhance mechanical properties.⁵ By regulating the parameters of the austempering treatment, the ultimate tensile strength can reach to 1400 MPa.⁶ Moreover, carbon partitioning treatment improved the ductility⁷ and cryogenic treatment promoted the transformation of austenite to martensite in ADI and improved its wear resistance.⁸

Alloying is another effective way to improve the mechanical properties of ductile iron.⁹ Various alloying elements, such as nickel (Ni),¹⁰ chromium (Cr),¹¹

manganese (Mn),¹² copper (Cu),¹³ cobalt (Co),¹⁴ and niobium (Nb),¹⁵ and their different combinations have been added to modify the microstructure. The addition of alloying elements usually improves strength by promoting carbide precipitation in as-cast conditions.¹⁶ Currently, studies focus on obtaining acicular structures, such as bainite and martensite, through alloying to enhance the mechanical properties.¹⁷ A cast ductile iron with an ausferrite matrix was produced by permanent mold casting in chromium-containing ductile iron.¹⁸ Less than 4% Ni is combined with Mo¹⁹ or Mn²⁰ to modify phase transformation processes and achieve acicular structures in ductile iron. Generally, a small amount of Ni is used to improve hardenability.²¹ When the Ni content in ductile iron exceeds 13%, an austenitic microstructure can be obtained and is widely utilized in corrosive environments.²² The previous investigations mainly focused on ductile irons with Ni content below 4% or above 13%, but there is very little research on the effects of intermediate nickel content on ductile iron's microstructure and mechanical properties.

In order to elucidate the effects of Ni content on the microstructure and mechanical properties of ductile iron, ductile iron with 0–10% Ni contents was produced by the horizontal continuous casting method. The casting

produced by the continuous casting process has fewer casting defects compared to sand casting.^{23,24} The phase constituents of ductile iron with various Ni contents were investigated in this study, in order to provide a reference for alloy design and property optimization of ductile iron.

Experimental Procedures

Ductile iron bars with a diameter of 100 mm were prepared in a horizontal continuous casting machine, which consists of a tundish, a mold, a roller table, a withdrawal mechanism, a water-cooling system, and a control system, as shown in Figure 1. The melting process was conducted in a medium-frequency induction furnace with a maximum holding capacity of 2000 kg and the tapping temperature was from 1450 to 1500 °C. Steel scrap, carbon additives, ferrosilicon, and nickel plates (99.0 wt% Ni) were used to adjust carbon, silicon, and nickel content, respectively. The Si-Mg-Ca-Ba spheroidization wire with a composition of 45.7 wt% Si, 23.4 wt% Mg, 3.6 wt% Ca, 2.4 wt% Ba and 2.3 wt% RE was employed for spheroidization treatments and Si-Ba-Mg-Ca inoculation wire with a composition of 64.5 wt% Si, 7.4 wt% Ba, 5.6 wt% Mg, 1.5 wt% Ca and 0.6 wt% RE was used for inoculation treatment in the present study. After spheroidization and inoculation treatments, the melt was transferred to a preheated holding furnace with a temperature range of 1260 °C to 1320 °C. When the melt flowed into the graphite mold, the casting process started at a drawing speed of 1.0 m/min.

Samples were taken from the cast bars in the position located about 10 mm from the edge for composition analysis, microstructure observation, and mechanical testing. The schematic diagram is presented in Figure 2.

The chemical compositions of samples were detected through a QSN-750 optical emission spectrometer, as shown in Table 1. Residual Mg content was determined by Avio-500 ICP emission-spectroscopy. Carbon equivalents were determined using the following equation:²⁵

$$\text{C.E.} = \text{C}\% + 0.33\text{Si}\% + 0.047\text{Ni}\% - (0.0055\text{Ni}\% \times \text{Si}\%) \quad \text{Eqn. 1}$$

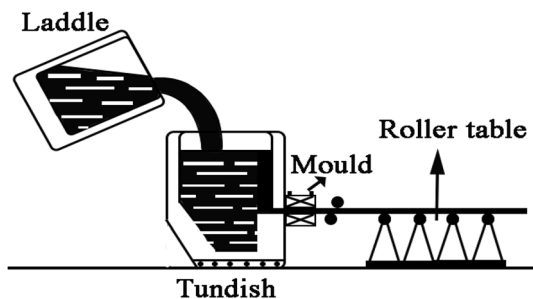


Figure 1. Schematic diagram of the horizontal continuous casting machine.

Based on the composition results, the samples were denoted as 0Ni, 2Ni, 4Ni, 6Ni, 8Ni, and 10Ni in the following sections. Annealing heat treatment was carried out in a vacuum furnace at 900 °C and held for 4h. Subsequently, the samples were furnace-cooled to ambient temperature.

Standard metallographic specimens were prepared through mechanical grinding, polishing, and etching with 4% nital solution. The microstructure was analyzed using an OLYMPUS GX71 optical microscope (OM) and a JSM-6700F scanning electron microscope (SEM) with an accelerating voltage of 30 kV. The graphite nodule count, volume fraction, and diameter were measured using ImageJ, a software for image analysis, on unetched OM images (at 200X) with at least 25 fields and a trap size of 5 µm to ensure statistical significance,²⁶ and ferrite grain size was measured on SEM images. The nodularity of graphite nodules was determined according to ASTM 247. A JEM-3010F transmission electron microscope (TEM) was used for transmission microstructure observation with an accelerating voltage of 300 kV. The TEM specimens were first mechanically polished, followed by twin-jet electropolishing in a solution of 95% perchlorate and 5% alcohol, and then ion-milled to remove the oxide layer. X-ray diffraction analyses were performed on an XRD-7000 diffractometer with a scanning range of 30°–90° and a scanning speed of 4°/min. A monochromatic Cu K α radiation with a wavelength (λ) of 1.5406 Å was used.

The tensile specimens with a cross-section of 4 mm \times 2 mm² and a gauge length of 20 mm were prepared. Tensile tests were conducted with an extensometer at room temperature using an HT-2402 universal testing machine with a 1 mm/min crosshead speed. Unnotched samples with 10 mm \times 10 mm \times 55 mm were used for Charpy impact tests using a JBN-300B impact testing machine, according to the ASTM E-23 standard. At least three tensile and impact tests were conducted on each type of Ni-containing

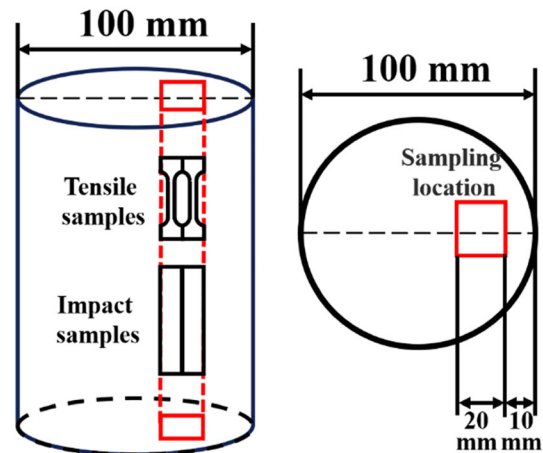


Figure 2. The schematic diagram for the samples taken from the cast bars.

Table 1. Chemical Composition of As-Cast Ductile Iron Samples with Different Ni Contents (wt%)

Element	0 wt% Ni	2 wt% Ni	4 wt% Ni	6 wt% Ni	8 wt% Ni	10 wt% Ni
C	3.40	3.44	3.45	3.38	3.39	3.37
Si	2.54	2.58	2.42	2.50	2.51	2.43
Mn	0.14	0.15	0.12	0.11	0.14	0.13
P	0.05	0.04	0.04	0.03	0.03	0.03
S	0.01	0.01	0.01	0.02	0.01	0.01
Ni	0.00	1.87	3.73	6.09	8.11	10.00
Mg	0.085	0.115	0.095	0.105	0.110	0.125
Cu	0.006	0.006	0.009	0.006	0.007	0.007
Cr	0.011	0.01	0.011	0.016	0.011	0.011
Mo	0.004	0.004	0.004	0.007	0.005	0.006
Al	0.018	0.016	0.016	0.018	0.016	0.014
RE	0.04	0.03	0.03	0.02	0.03	0.03
CE	4.24	4.35	4.37	4.41	4.49	4.50

specimen to ensure repeatability. The fracture morphology was analyzed via SEM. Hardness tests were carried out using an HVT-1000 microhardness tester with a load of 100 g and a holding time of 15 s. At least 10 points were obtained, and the average value was determined.

Results

Effects of Ni Content on the Microstructure of As-Cast Ductile Iron

Figure 3 shows the unetched OM images of as-cast ductile iron samples with different Ni contents. It could be seen that the spheroidal graphite was uniformly distributed around the matrix with high nodularity. The addition of 2% Ni increased the graphite nodule count but reduced the graphite diameter. When further increasing Ni addition, the graphite nodule count was decreased and the graphite diameter was slightly increased.

The variations in the graphite nodule count, volume fraction, nodularity, and diameter are presented in Figure 4. The addition of 2% Ni increased the graphite nodule count, volume fraction, and nodularity. However, further increasing Ni content showed the opposite effect. When the Ni content increased from 2 to 10%, the graphite nodule count decreased from 782 to 545/mm², graphite fraction decreased from 10.5 to 8.8%, and the nodularity decreased from 97 to 94%, respectively. It was worth noting that Ni addition increased the graphite nodules and improved nodularity.

Figure 5 shows the SEM images of as-cast ductile iron samples with different Ni contents. It could be seen that the samples with different Ni contents showed obvious distinct matrix microstructures. All samples showed a small amount of carbide in the matrix due to the high undercooling. The ductile iron with Ni amounts less than 2% showed a ferritic matrix. With the increase of Ni addition, the phase fraction changed. The 4Ni sample showed more than 40% pearlite (Figure 5c), and bainite and martensite were observed in the samples containing 6%, 8%, and 10% Ni (Figure 5d–f). Moreover, the martensite fraction was increased with increasing Ni content. It indicated that Ni addition in ductile iron affected the phase transformation during solid-state transformation after solidification.

Figure 6 illustrates the XRD patterns of as-cast ductile iron samples with different Ni contents. The (110), (200), and (211) planes of α -phase were detected for all samples, while when the Ni content exceeded 6%, (111), (002), and (113) planes of γ phase were also detected. As ferrite, bainite, and martensite diffraction peaks were located in similar positions, it wasn't easy to differentiate the phase from the α -phase's peaks. However, compared with low Ni samples (0Ni, 2Ni, and 4Ni samples), the peaks of the α -phase of samples with high Ni contents (6Ni, 8Ni, and 10Ni samples) were much wider, indicating that the α -phase in these samples contained a certain range of carbon atoms. Combined with morphology observation, it could be inferred that the α -phase in high Ni samples contained ferrite, bainite, and martensite. Moreover, it could be found that the peaks of the γ phase were intensified with increasing Ni content, indicating that Ni addition hindered

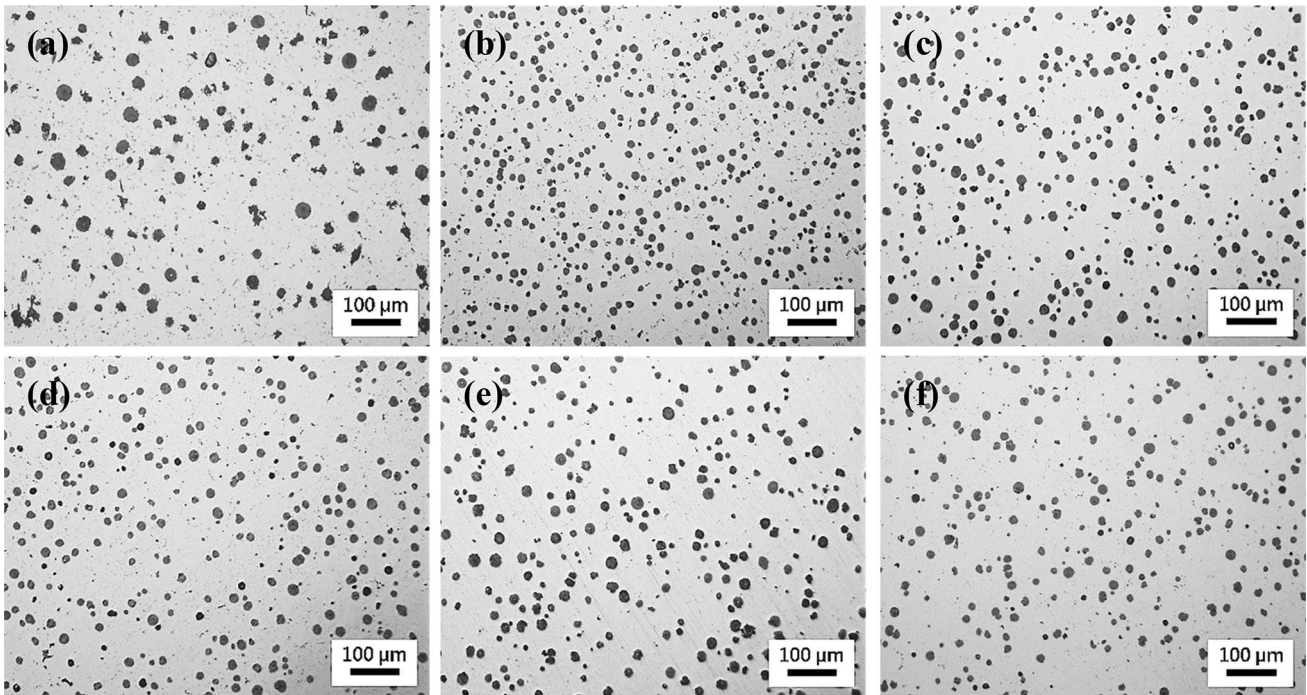


Figure 3. Unetched OM images of the as-cast ductile iron samples with different Ni contents: (a) 0Ni, (b) 2Ni, (c) 4Ni, (d) 6Ni, (e) 8Ni, (f) and 10Ni.

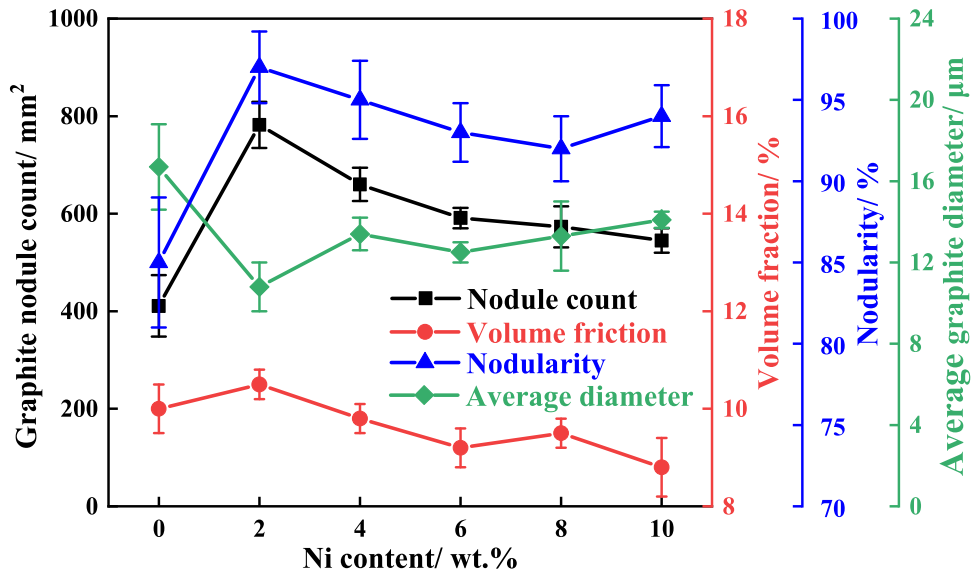


Figure 4. The graphite nodule count, volume fraction, nodularity, and diameter variations of ductile iron with different Ni contents.

the phase transformation of austenite. It was reported that Ni delayed austenite transformation in ADI.¹³

Effects of Ni Contents on the Microstructure of Ductile Iron After Annealing Treatment

Figure 7 shows the SEM images of as-annealed ductile iron samples with different Ni contents. It could be clearly seen that the carbides that existed in the castings were

eliminated. After annealing treatment, the ferrite matrix was detected for the 0Ni, 2Ni, and 4Ni samples. Furthermore, the as-annealed 2Ni sample showed a finer ferrite size of 19 μm than the as-annealed 4Ni sample of 24 μm and as-annealed 0Ni sample of 41 μm. The ferrite phase was nucleated first at the interface of austenite/graphite; thus, more graphite nodules in the 2Ni sample provided more nucleation sites and refined ferrite grain size.²⁷ For the as-annealed 6Ni and 8Ni samples, part of the matrix microstructure transformed into ferrite. Additionally, the

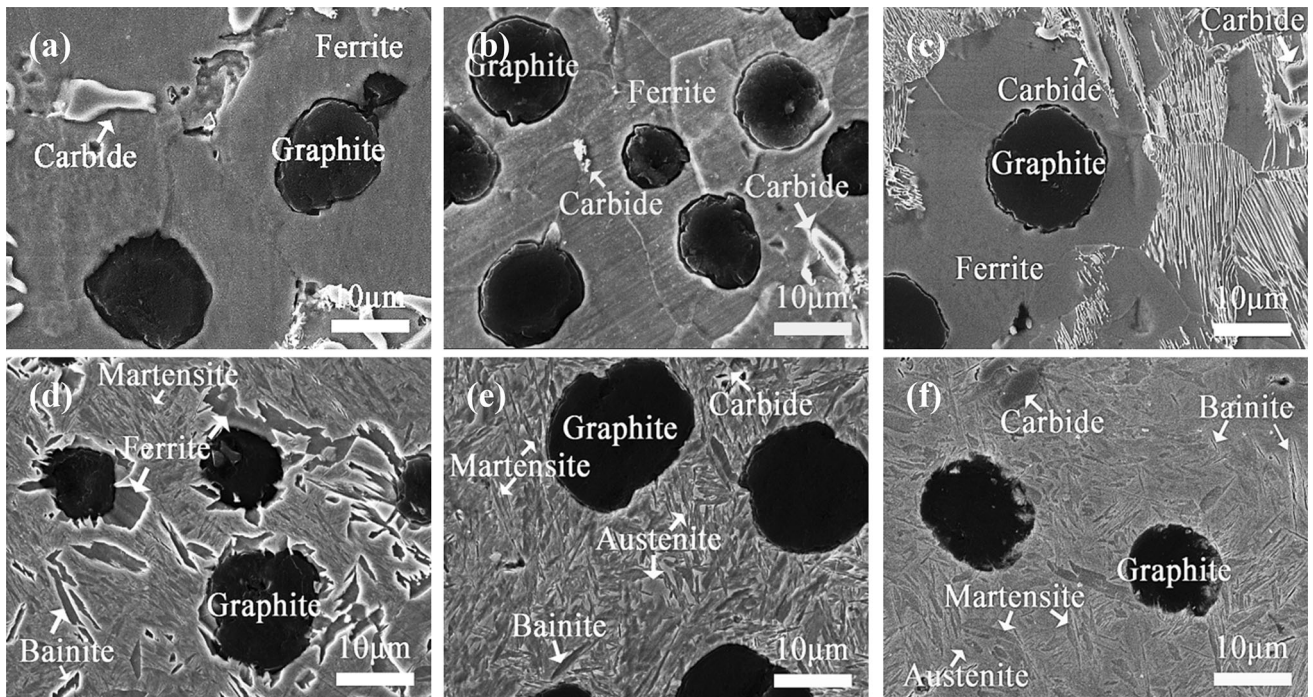


Figure 5. SEM images of the as-cast ductile iron samples with different Ni contents: (a) 0Ni, (b) 2Ni, (c) 4Ni, (d) 6Ni, (e) 8Ni, (f) and 10Ni.

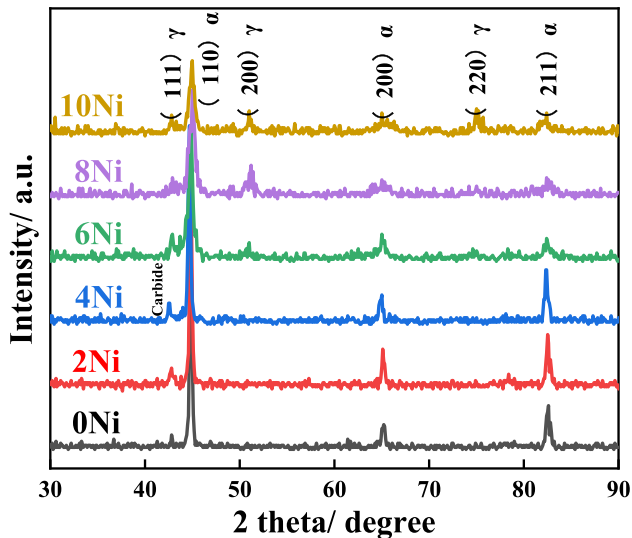


Figure 6. XRD patterns of as-cast ductile iron samples with different Ni contents.

as-annealed 6Ni sample contained more ferrite than the 8Ni sample. However, no ferrite was detected in the as-annealed 10Ni sample, whose microstructure was similar to the as-cast 10Ni sample, indicating that austenite was mainly transformed into martensite even with a very slow cooling rate. Moreover, due to the higher cooling rate, the as-cast 10Ni sample showed finer acicular structures than the as-annealed 10Ni sample.

Figure 8 illustrates the XRD patterns of as-annealed ductile iron samples with different Ni contents. The carbide peaks

disappeared, indicating that carbides were dissolved in the matrix during annealing. Additionally, the height of the γ phase peak of as-annealed samples showed a similar trend with as-cast samples, indicating that the austenite fraction increased with increasing Ni content.

In this study, the volume fraction of α -phase and γ phase in high Ni samples was estimated via direct comparison by determining the peak intensities of $(111)\gamma$, $(200)\gamma$, $(220)\gamma$, $(110)\alpha$, $(200)\alpha$, and $(211)\alpha$.²⁸ Additionally, the ferrite, pearlite, and carbide volume fractions were determined via ImageJ software on SEM images. At least twenty-five fields were selected to determine the values. The structures exhibited in as-cast and as-annealed ductile iron samples with different Ni contents were estimated and shown in Figure 9. It could be seen that the matrix, with increasing Ni content, gradually transformed from ferrite to pearlite and then to bainite and martensite. Moreover, the volume fraction of austenite was increased with the increase of Ni addition because Ni addition had the ability to stabilize austenite.²⁹

Effects of Ni Content on the Mechanical Properties of Ductile Iron

Figure 10 shows the typical tensile stress-strain curves of ductile iron samples, and related mechanical properties are listed in Table 2. The variations of ultimate tensile strength (UTS) and hardness of ductile iron samples with different Ni contents are presented in Figure 11. After annealing

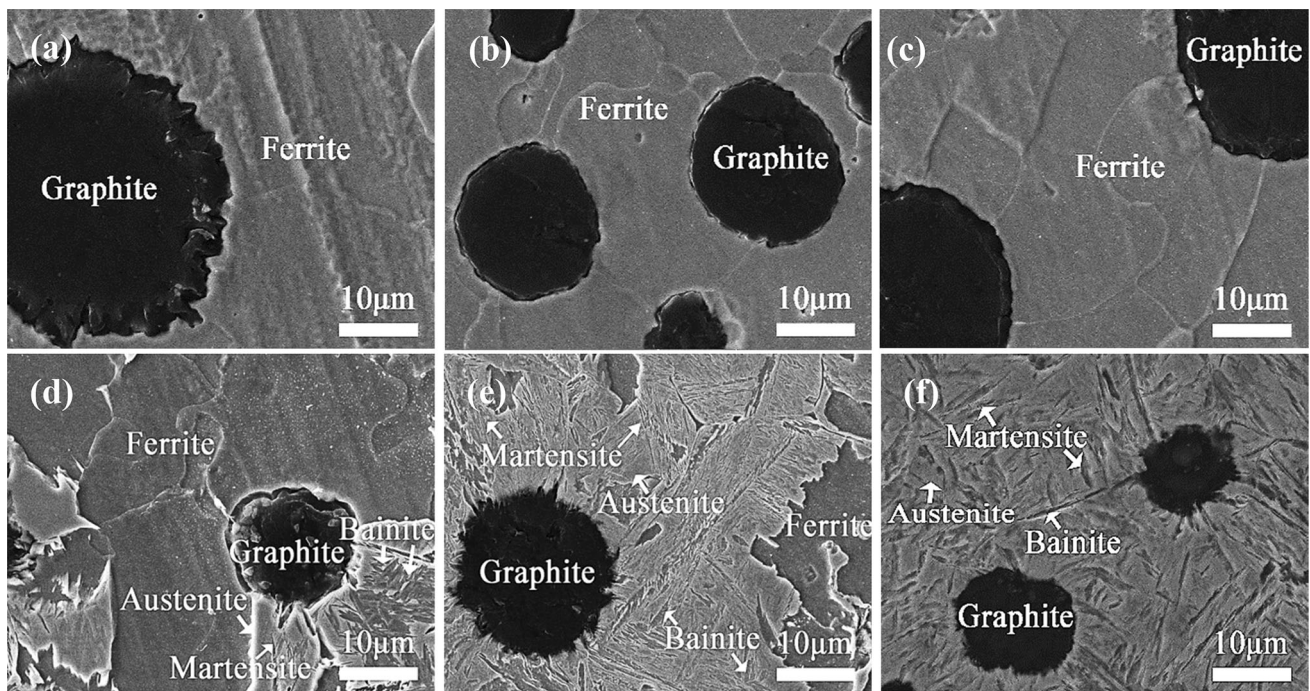


Figure 7. SEM images of the as-annealed ductile iron samples with different Ni contents: (a) 0Ni, (b) 2Ni, (c) 4Ni, (d) 6Ni, (e) 8Ni, (f) and 10Ni.

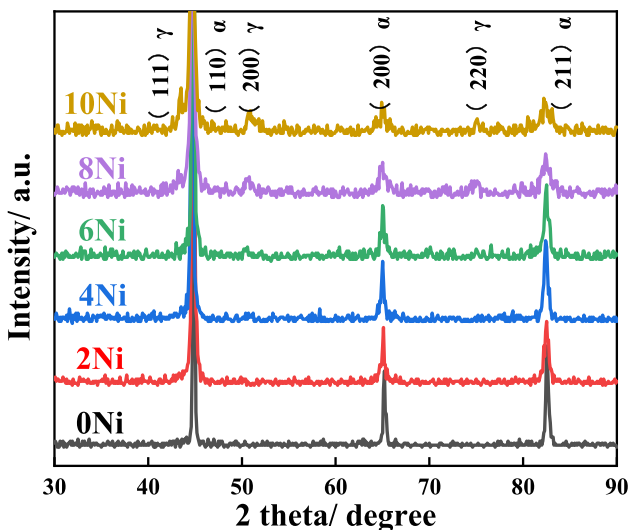


Figure 8. XRD patterns of as-annealed ductile iron samples with different Ni contents.

heat treatment, the UTS of ductile iron samples decreased. In addition, the hardness and strength increased with increasing Ni content. When the Ni content increased from 0 to 10%, the UTS increased from 467 to 1186 MPa for the as-cast samples, and the UTS increased from 466 to 1173 MPa for the as-annealed samples, respectively. Correspondingly, the hardness had a great increase with the increase of Ni content. Although finer martensitic grains gave higher yield strength, the release of stress after annealing reduced brittleness and gave rise to high ductility.³⁰ There were two sharp increases in strength, one of

which was when the Ni content increased from 4 to 6% for as-cast samples, and the other was when the Ni content increased from 6 to 8% for the as-annealed samples, corresponding to the formation of acicular structures.

Figure 12 shows the impact energy and total elongation (TL) variations of ductile iron samples with different Ni contents. Annealed samples exhibited better ductility than as-cast samples due to the elimination of carbides and reduction of dislocation density.³¹ With increasing Ni content, the ductility of samples first increased and then decreased. The TL of as-cast and as-annealed ductile iron samples without alloying increased from 12.0 to 12.9% and 16.5 to 18.2% with the addition of 2% Ni, respectively. Further increasing Ni content to 10%, the TL decreased to 2.2% and 2.4% for the as-cast and as-annealed condition, which should be related to the formation of brittle acicular structures. The impact energy of the ductile iron has a similar trend with elongation.

Figure 13 shows the tensile fracture surfaces of as-annealed ductile iron samples with different Ni content. Graphite and graphite cavities were observed on fracture surfaces. Moreover, quasi-cleavage facets and dimples were found in specimens, which were indicators of ductile and brittle features, respectively.³² The as-annealed 0Ni, 2Ni, and 4Ni samples showed a large number of dimples, corresponding to high ductility. For the as-annealed 6Ni sample, quasi-cleavage facets with dimples were found, corresponding to a typical mixed fracture mode. However, the fracture surfaces of as-annealed 8Ni and 10Ni samples showed a large amount of quasi-cleavage facets and exhibited brittleness.

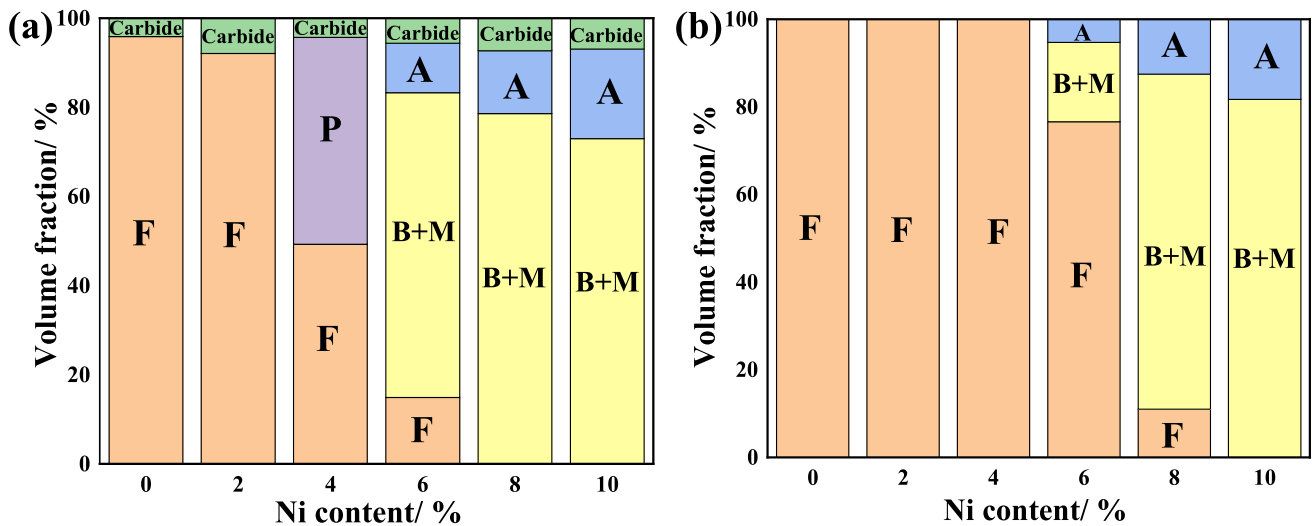


Figure 9. Structures in (a) as-cast and (b) as-annealed ductile iron samples with different Ni contents.

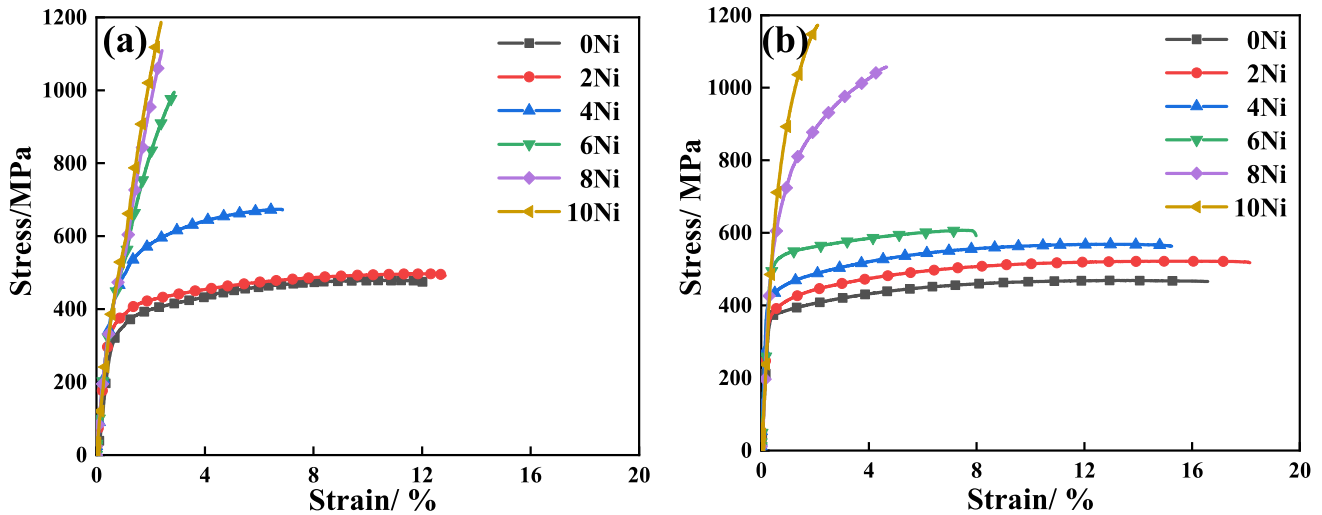


Figure 10. Tensile stress-strain curves of (a) as-cast and (b) as-annealed ductile iron samples with different Ni contents.

Discussion

Microstructure Evolution of Ductile Iron with Different Ni Contents

Ni is an essential graphitizing element and previous investigation has indicated that 2% Ni addition increased graphite nodule count and nodularity, but further addition had the opposite effect.²² During solidification, graphite first nucleated from the melt, including hypereutectic graphite that directly nucleated from the melt with a large diameter and a small count and eutectic graphite that nucleated during eutectic reactions with a small diameter and a large count.^{33,34} The hyper, hypo, or eutectic was determined by carbon equivalents (CE), which modified the solidification process during eutectic reactions.³⁵ In this study, the CE value of Ni-containing ductile iron increased with increasing Ni content. High CE% commonly

corresponded to more graphite nodules,²² thus Ni addition increased the CE% value, which was beneficial for the increase of graphite nodules. In addition, Ni addition expanded the temperature interval of the eutectic solidification and then promoted the precipitation of graphite nodules from the melt during solidification. However, when the Ni content exceeded 2%, more Ni atoms replacing Fe atoms increased the diffusion activation energy of carbon atoms in austenite, thus inhibiting the diffusion of carbon atoms.³⁶ As a result, the graphite was decreased for further increase of Ni addition. Lacking carbon depletion, the austenite with high carbon content finally transformed into pearlite or acicular structures. Therefore, the 2Ni sample with a ferrite matrix showed a higher graphite fraction and more graphite nodules than the 4Ni sample with a high pearlite fraction. It has also shown that more Ni addition in ductile iron gave rise to the reduction of graphite nodules.²⁰ Based on the two opposite

Table 2. Mechanical Properties of the As-Cast and As-Annealed Ductile Iron Samples with Different Ni Contents

	Ultimate tensile strength/MPa	Yield strength/MPa	Total elongation/%	Hardness/ Hv	Impact energy/J
<i>As-cast condition</i>					
0Ni	467	335	12.0	213.6	107
2Ni	491	364	12.9	234.6	114
4Ni	672	479	6.9	321.2	52
6Ni	995	753	2.9	498.4	32
8Ni	1108	1018	2.4	598.4	22
10Ni	1186	1105	2.2	584.5	20
<i>As-annealed condition</i>					
0Ni	466	352	16.5	181.7	143
2Ni	521	383	18.2	229.4	149
4Ni	568	421	15.2	249.8	78
6Ni	607	519	8.0	307.4	65
8Ni	1057	656	4.6	553.5	35
10Ni	1173	896	2.4	578.2	22

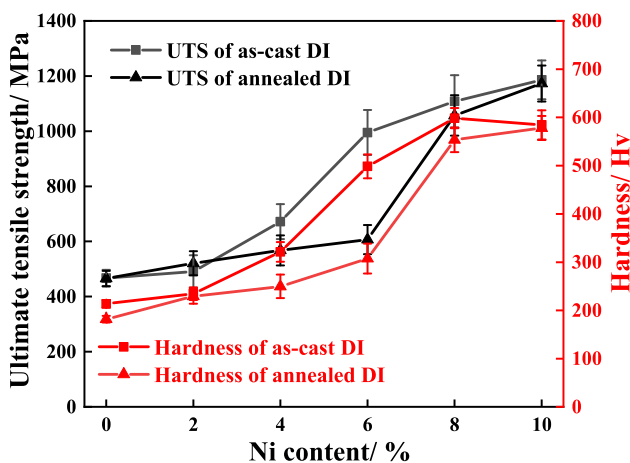


Figure 11. Variations of strength and hardness of ductile iron samples with different Ni contents.

effects of Ni on the formation of graphite, the graphite amounts for the ductile iron with different Ni contents varied little. It should be noted that high residual Mg content existed in the samples, which might be related to the spheroidization and inoculation treatments during fabrication. This might be the reason of the nodularity variation in samples with different Ni contents.

The diffusion of carbon atoms determined the phase transformation process. During the solid-state transformation of 0Ni and 2Ni samples, carbon atoms diffused to graphite, forming a ferrite matrix. With increasing Ni content, solute Ni hampered the carbon diffusion from the austenite to the graphite nodules. It led to the formation of pearlite in regions far from graphite. Watsada et al.¹⁰ obtained a full pearlite matrix when increasing Ni content

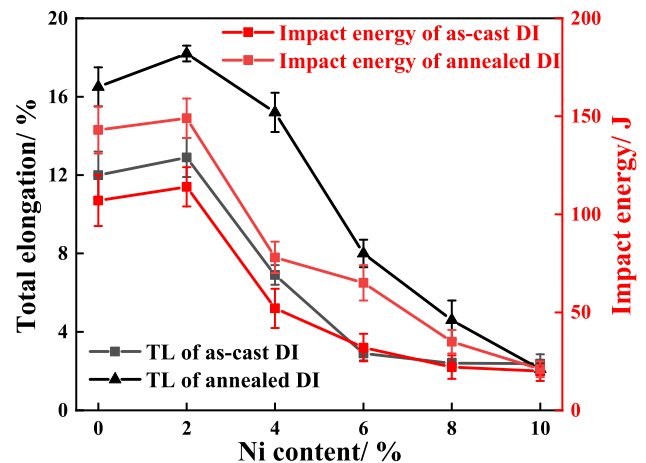


Figure 12. Variations of TL and impact energy of ductile iron samples with different Ni contents.

to 4.5 wt%. Further increasing Ni content, more Ni atoms substituted Fe atoms, which made it more difficult for carbon atoms to diffuse. Lacking substantial carbon depletion, the austenite with high lattice distortion finally transformed into bainite and martensite during solid-state transformation. In addition, the martensite fraction was increased with increasing Ni content. As a result, although ductile irons with the same diameter had similar cooling rates during the casting, different Ni additions exhibited different carbon diffusivities, resulting in various phase constituents. When acicular structures were generated, retained austenite was preserved in the matrix and could be detected by XRD.³⁷

Annealing treatment could eliminate carbides and segregation (Figure 6a), making the microstructure more

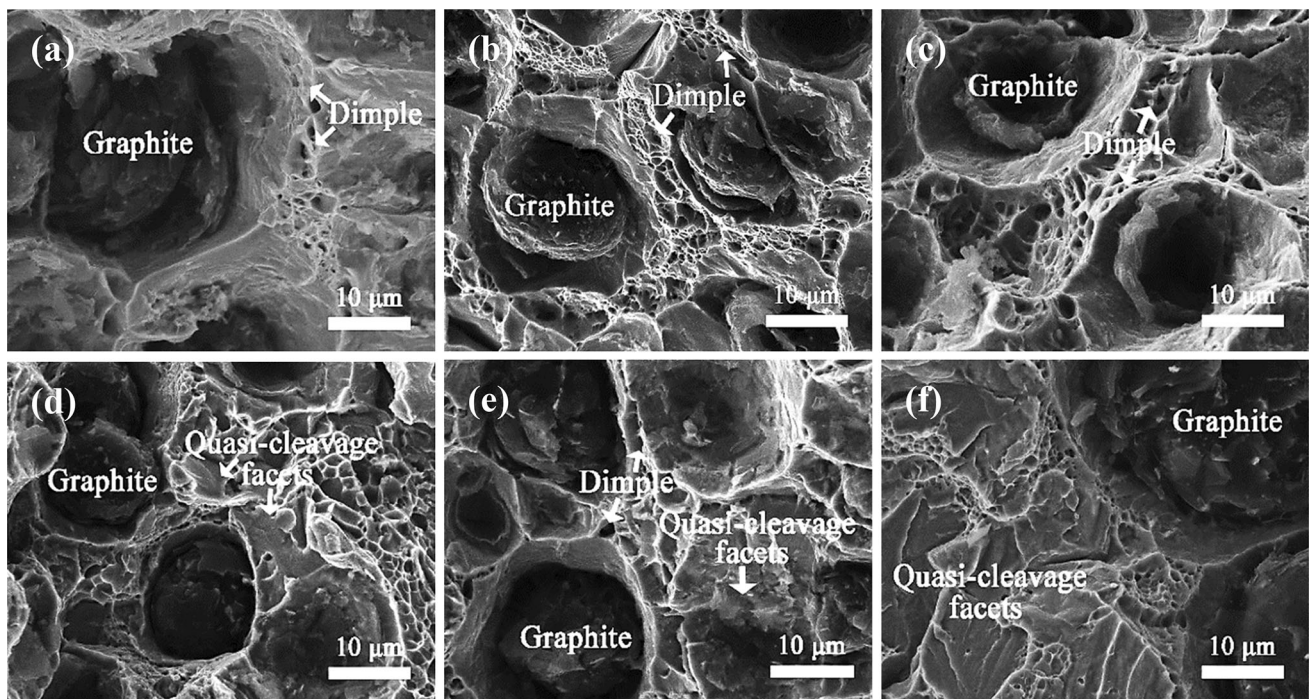


Figure 13. Fracture surfaces of as-annealed ductile iron samples with different Ni contents: (a) 0Ni, (b) 2Ni, (c) 4Ni, (d) 6Ni, (e) 8Ni, (f) and 10Ni.

Table 3. Q Values of Ductile Irons with Different Ni Contents ($\times 10^6$)

	0Ni	2Ni	4Ni	6Ni	8Ni	10Ni
As-cast	2.7	3.1	3.1	2.8	2.4	2.1
As-annealed	3.6	4.9	4.9	2.9	5.2	3.3

uniform. Moreover, the slow cooling rate during annealing allowed more carbon atoms to diffuse into graphite. Consequently, compared to the cast sample, the ferrite fraction of the annealed sample increased. However, the 6Ni and 8Ni samples with low carbon diffusivity led to the transformation of some austenite into acicular structures even at a slow cooling rate. For the 10Ni sample, the diffusion of carbon atoms was almost prohibited. Consequently, a similar microstructure was obtained for the as-cast and as-annealed samples.

Mechanical Properties Analysis of Ductile Iron with Different Ni Contents

The ductile iron samples with different Ni contents exhibited different mechanical responses. The as-cast 0Ni, 2Ni, and as-annealed 0Ni, 2Ni, 4Ni, and 6Ni samples showed similar UTS attributed to the ferrite matrix. Higher Ni content gave rise to better solution strengthening and higher strength. Further increasing Ni content led to the formation of acicular structures, and this gave rise to a sharp increase in strength. Thus, the strengths were

improved significantly when the Ni content increased from 4 to 6% and 6 to 8% for the as-cast and as-annealed samples, respectively. Correspondingly, brittle acicular structures deteriorated ductility.

The comprehensive performance of ductile iron was calculated using the following equation:³⁸

$$Q = \text{tensile strength}^2 \times \text{elongation} \quad \text{Eqn. 2}$$

where Q represents the performance of ductile iron; that is, a larger Q value represents a higher tensile performance. The Q values of ductile irons with different Ni content in this study are listed in Table 3. The results showed that the as-annealed samples showed better mechanical properties because of the elimination of carbides and improvement of microstructure uniformity.³⁹ This was worth noting that the 2Ni sample, whether for the as-cast or as-annealed condition, showed higher mechanical properties than ductile iron without alloying. It was because the 2Ni sample exhibited finer grain size and more graphite nodules with higher nodularity, which reduced the stress concentration at the matrix/graphite interface and delayed

the onset of cracking.^{40,41} The Q values of ADI produced by different austempering processes ranged from 2.3 to 5.6×10^6 .⁶ In this study, the as-annealed 8Ni sample exhibited similar mechanical properties.

Conclusions

In the present study, the effects of Ni addition on the microstructure and mechanical properties of the as-cast and as-annealed ductile iron were investigated. The main conclusions were summarized as follows.

1. Ni addition had a significant effect on the microstructure of ductile iron. 2% Ni addition increased the graphite nodule count, whilst the graphite nodule count was reduced for further increase of Ni content.
2. The matrix of the samples with Ni content no more than 2% was mainly composed of ferrite, and pearlite was detected for 4% Ni contained sample. Further increase of Ni content resulted in the formation of acicular microstructure.
3. Carbides was dissolved into the matrix through annealing treatment. Consequently, a ferrite matrix was obtained for samples with Ni contents no more than 4%.
4. For 6Ni and 8Ni samples, the retained austenite partly transformed into ferrite and partly into acicular structures during annealing treatment. However, the microstructure changed little for the sample with 10% Ni because of the slow diffusion of carbon atoms.
5. As the Ni content increased, the strength of as-cast ductile iron increased but the ductility decreased, which was closely related to the phase constituents.
6. Annealing treatment improved the ductility of Ni-containing ductile iron significantly due to the reduction of carbides or the homogenous microstructure.

Acknowledgement

This work was supported by the China Postdoctoral Science Foundation-funded project (Nos. 2019M653703 and 2020T130523).

Data Availability

The raw/processed data required to reproduce these findings cannot be shared at this time due to technical or time limitations.

REFERENCES

1. W. Stets, H. Löblich, G. Gassner, P. Schumacher, Solution strengthened ferritic ductile cast iron

- properties, production and application. *Inter Metalcast.* **8**(2), 35–40 (2014). <https://doi.org/10.1007/BF03355580>
2. J.L. Hernández-Rivera, R.E. Campos Cambranis, A. de la Garza, Study of microstructural evolution and mechanical properties exhibited by non alloyed ductile iron during conventional and stepped austempering heat treatment. *Mater. Des.* **32**(10), 4756–4762 (2011)
3. R. Gundlach, Normalizing heat treatments to develop improved properties in heavy section ductile iron. *Ductile Iron Soc. Res. Rep.* **48**, 217–223 (2014)
4. R.B. Gundlach, Heat treatments to develop high-strength ferritic ductile iron. *Inter Metalcast.* **14**(4), 1065–1077 (2020). <https://doi.org/10.1007/s40962-020-00489-0>
5. S.K. Putatunda, S. Kesani, R. Tackett, G. Lawes, Development of austenite free ADI (austempered ductile cast iron). *Mater. Sci. Eng. A* **435–436**, 112–122 (2006)
6. X. Wang, Y. Du, C. Liu, Relationship among process parameters, microstructure, and mechanical properties of austempered ductile iron (ADI). *Mater. Sci. Eng. A* **857**, 144063 (2022)
7. X. Wang, Y. Du, B. Liu, B. Jiang, Enhanced plasticity of austempered ductile iron (ADI) by partitioning treatment. *Mater. Sci. Eng. A* **804**, 140513 (2021)
8. F.H. Çakir, The effect of cryogenic treatment on hardness, toughness, and tribological properties of austempered ductile iron with different nickel contents. *Inter Metalcast.* **16**(3), 1442–1454 (2022). <https://doi.org/10.1007/s40962-021-00686-5>
9. S. Biswas, C. Monroe, T. Prucha, Use of published experimental results to validate approaches to gray and ductile iron mechanical properties prediction. *Inter Metalcast.* **11**(4), 656–674 (2017). <https://doi.org/10.1007/s40962-016-0126-3>
10. W. Siripongtana, R. Canyook, Influence of nickel on the microstructure and mechanical properties of nodular cast iron. *Mater. Sci. Forum* **1023**, 61–66 (2021)
11. A. ElJersifi, K. Aouadi, M. Ben Ali, A. Chbihi, The effect of heat treatments on the properties of a ferritic high-chromium cast iron. *J. Mater. Eng. Perform.* **32**(18), 8262–8273 (2023)
12. J. Lacaze, J. Sertucha, Effect of Cu, Mn and Sn on pearlite growth kinetics in as-cast ductile irons. *Int. J. Cast Met. Res.* **29**(1–2), 74–78 (2016)
13. U. Batra, S. Ray, S.R. Prabhakar, The influence of nickel and copper on the austempering of ductile iron. *J. Mater. Eng. Perform.* **13**(1), 64–68 (2004)
14. A. Almanza, D. Dewald, J. Licavoli, P.G. Sanders, Influence of cobalt in the tensile properties of ½ inch ductile iron Y-blocks. *Inter Metalcast.* **15**(2), 433–446 (2020). <https://doi.org/10.1007/s40962-020-00521-3>
15. X. Chen, J. Xu, H. Hu, H. Mohrbacher, Effects of niobium addition on microstructure and tensile behavior of as-cast ductile iron. *Mater. Sci. Eng. A* **688**, 416–428 (2017)

16. J.M. Tartaglia, R.B. Gundlach, G.M. Goodrich, Optimizing structure–property relationships in ductile iron. *Inter Metalcast.* **8**(4), 7–38 (2014). <https://doi.org/10.1007/BF03355592>
17. S.C. Murcia, M.A. Paniagua, E.A. Ossa, Development of as-cast dual matrix structure (DMS) ductile iron. *Mater. Sci. Eng. A* **566**, 8–15 (2013)
18. J.-P. Zou, K. Shimizu, Q.-Z. Cai, Effects of Cr content and annealing temperature on microstructure and wear characteristics of cast ausferrite nodular iron. *J. Iron. Steel Res. Int.* **22**(11), 1049–1054 (2015)
19. S.M.M. Kashani, S.M.A. Boutorabi, As-cast acicular ductile aluminum cast iron. *J. Iron. Steel Res. Int.* **16**(6), 23–28 (2009)
20. T. Nobuki, M. Hatate, T. Shiota, Mechanical characteristics of spheroidal graphite cast irons containing Ni and Mn with mixed ferrite and bainitic ferrite microstructure. *Int. J. Cast Met. Res.* **21**(1–4), 31–38 (2008)
21. S.K. Yu, C.R. Loper Jr, H.H. Cornell, Effect of molybdenum, copper and nickel in the microstructure, hardness, and hardenability of ductile cast irons. *Trans. Am. Foundrymen's Soc.* **94**, 557–576 (1987)
22. N. Fatahalla, A. AbuElEzz, M. Semeida, C. Si and Ni as alloying elements to vary carbon equivalent of austenitic ductile cast iron: microstructure and mechanical properties. *Mater. Sci. Eng. A* **504**(1), 81–89 (2009)
23. P. Chaengkham, P. Srichandr, Continuously cast ductile iron: processing, structures, and properties. *J. Mater. Process. Technol.* **211**(8), 1372–1378 (2011)
24. P.R. Gangasani, Evaluation of fatigue strengths of continuously cast ductile irons. *Inter Metalcast.* **1**(1), 41–55 (2007). <https://doi.org/10.1007/BF03355417>
25. M. Henderson, *Ductile iron handbook*, AKS. Des Plaines (1992) 167.
26. S. Grenier, C. Labrecque, A. Bhattacharjee, R. Gundlach, B. Kroka, M. Riabov, Inter-laboratory study of nodularity and nodule count of ductile iron by image analysis. *Inter Metalcast.* **8**(2), 51–63 (2014). <https://doi.org/10.1007/BF03355582>
27. H.D. Machado, R. Aristizabal-Sierra, C. Garcia-Mateo, I. Toda-Caraballo, Effect of the starting microstructure in the formation of austenite at the intercritical range in ductile iron alloyed with nickel and copper. *Inter Metalcast.* **14**(3), 836–845 (2020). <https://doi.org/10.1007/s40962-020-00450-1>
28. C. Roberts, Effect of carbon on the volume fractions and lattice parameters of retained austenite and martensite. *JOM* **5**, 203–204 (1953)
29. D. De Knijf, R. Petrov, C. Föjer, L.A.I. Kestens, Effect of fresh martensite on the stability of retained austenite in quenching and partitioning steel. *Mater. Sci. Eng. A* **615**, 107–115 (2014)
30. R. Aristizabal, R. Foley, A. Druschitz, Intercritically austenitized quenched and tempered ductile iron. *Inter Metalcast.* **6**(4), 7–14 (2012). <https://doi.org/10.1007/BF03355534>
31. K. Kocatepe, M. Cerah, M. Erdogan, The tensile fracture behaviour of intercritically annealed and quenched+tempered ferritic ductile iron with dual matrix structure. *Mater. Des.* **28**(1), 172–181 (2007)
32. J. Zhao, B. Lv, F. Zhang, Z. Yang, L. Qian, C. Chen, X. Long, Effects of austempering temperature on bainitic microstructure and mechanical properties of a high-C high-Si steel. *Mater. Sci. Eng. A* **742**, 179–189 (2019)
33. H. Nakae, S. Jung, T. Kitazawa, Eutectic solidification mode of spheroidal graphite cast iron and graphitization. *China Found.* **4**, 33 (2007)
34. B. Bauer, I. Mihalic Pokopec, M. Petrič, P. Mrvar, Effect of cooling rate on graphite morphology and mechanical properties in high-silicon ductile iron castings. *Inter Metalcast.* **14**(3), 809–815 (2020). <https://doi.org/10.1007/s40962-020-00432-3>
35. J. Lacaze, S. Armendariz, P. Larrañaga, I. Asenjo, J. Sertucha, R. Suárez, Effect of carbon equivalent on graphite formation in heavy-section ductile iron parts. *Mater. Sci. Forum* **636–637**, 523–530 (2010)
36. L.G. Wang, C.Y. Wang, First-principles calculations of energies of impurities and doping effects at grain boundaries in nickel. *Mater. Sci. Eng. A* **234–236**, 521–524 (1997)
37. M.J. Peet, S.S. Babu, M.K. Miller, H.K.D.H. Bhadeshia, Tempering of low-temperature bainite. *Metall. Mater. Trans. A* **48**(7), 3410–3418 (2017)
38. W. Siefert, K. Orth, Evaluation of ductile iron in terms of feasible properties of the material. *Trans. Am. Foundrymen's Soc.* **78**, 155–161 (1970)
39. S.Y. Han, S.Y. Shin, H.-J. Lee, B.-J. Lee, S. Lee, N.J. Kim, J.-H. Kwak, Effects of annealing temperature on microstructure and tensile properties in ferritic lightweight steels. *Metall. Mater. Trans. A* **43**(3), 843–853 (2012)
40. C. Liu, Y. Du, X. Wang, T. Ying, L. Zhang, X. Zhang, G. Yan, B. Jiang, Effects of graphite nodule count on mechanical properties and thermal conductivity of ductile iron. *Mater. Today Commun.* **31**, 103522 (2022)
41. A. Almanza, D. Dewald, J. Licavoli, P.G. Sanders, Effect of cobalt additions on the microstructure and mechanical properties of as-cast thin-wall ductile iron. *Inter Metalcast.* **15**(2), 417–432 (2021). <https://doi.org/10.1007/s40962-020-00513-3>

Publisher's Note Springer Nature remains neutral with regard to jurisdictional claims in published maps and institutional affiliations.

Springer Nature or its licensor (e.g. a society or other partner) holds exclusive rights to this article under a publishing agreement with the author(s) or other rightsholder(s); author self-archiving of the accepted manuscript version of this article is solely governed by the terms of such publishing agreement and applicable law.